

Received June 20, 2019, accepted July 7, 2019, date of publication July 15, 2019, date of current version August 1, 2019.

Digital Object Identifier 10.1109/ACCESS.2019.2928580

Real-Time Monitoring of Contact Impedance From Multiple Electrode–Scalp Interfaces During Cerebral Electrical Impedance Tomography

HANG MA^{ID}, HAOTING LI^{ID}, XUECHAO LIU, WEICHEN LI^{ID}, JUNYING XIA^{ID}, BENYUAN LIU^{ID}, XUETAO SHI^{ID}, XIUZHEN DONG, (Member, IEEE), AND FENG FU^{ID}

School of Biomedical Engineering, Air Force Medical University, Xi'an 710032, China

Corresponding authors: Xiuzhen Dong (dongxiuzhen@fmmu.edu.cn) and Feng Fu (fengfu@fmmu.edu.cn)

This work was supported in part by the Project of the National Natural Science Foundation of China under Grant 51837011, and in part by the National Natural Science Foundation of China under Grant 61571445.

ABSTRACT Electrical impedance tomography (EIT) is a promising medical technique for monitoring brain injury through the reflection of electrical impedance changes in internal brain tissues. However, the contact impedances at the electrode–scalp interfaces can still notably affect the EIT accuracy. Hence, we propose a method for real-time monitoring the multi-channel contact impedances of cerebral EIT using a reference electrode attached close to the head vertex. This method allows to approximate inter-channel differences and changes over time of multi-channel contact impedances. The experimental results on 36 volunteers show that the maximum relative inter-channel difference obtained from 16 disposable surface electrodes reaches 18.7%, and the maximum relative change over time reaches 19.2%. The proposed method can assist clinicians in real-time monitoring of contact conditions from the multiple electrode–scalp interfaces during the clinical application of the cerebral EIT.

INDEX TERMS Contact impedance, electrical impedance tomography, electrode–scalp interface.

I. INTRODUCTION

Electrical impedance tomography (EIT) is a functional imaging technique in which electrodes are attached to a region of the human body. Then, excitation currents are injected into the region through some of the electrodes for measuring the resulting voltage signals at relevant electrodes, and the spatial distribution of either electrical conductivities or their variation is imaged [1], [2]. EIT is promising for clinical diagnostics. For instance, it is sensitive to brain tissue damage resulting from cerebral hemorrhage, edema, and ischemia, and provides a high temporal resolution [3], [4]. In addition, the clinical implications of time-difference EIT have been demonstrated for monitoring brain injury [5]–[20].

The contact impedance of each electrode is a major factor affecting the accuracy of cerebral EIT [21]. During imaging, multiple electrodes are attached to the scalp, and their contact impedances at the electrode–scalp interface may differ and vary over time. Both variations may affect signal

acquisition accuracy and the resulting quality of the reconstructed EIT image [22]–[26]. Thus, real-time monitoring of the impedances on the multiple electrode–skin interfaces can allow to assess the reliability of the signals and images obtained from cerebral EIT.

The contact impedance in EIT is usually estimated using the two-electrode method, which is easy to apply and retrieves rough estimates of the contact quality at the electrode–skin interface. However, this method is inaccurate for real-time monitoring of the change over time on multi-channel contact impedances [27]. Currently, there is no method available to monitor in real time the inter-channel differences and change over time of multi-channel contact impedances. More specifically, no study has been conducted on the magnitudes of these changes considering contact impedances from the electrode–scalp interfaces during cerebral EIT. Although accurately measuring the electrode–skin contact impedance is challenging, real-time monitoring of inter-channel differences and change over time on multi-channel contact impedances for cerebral EIT can improve signal acquisition and the resulting images.

The associate editor coordinating the review of this manuscript and approving it for publication was Abdallah Kassem.

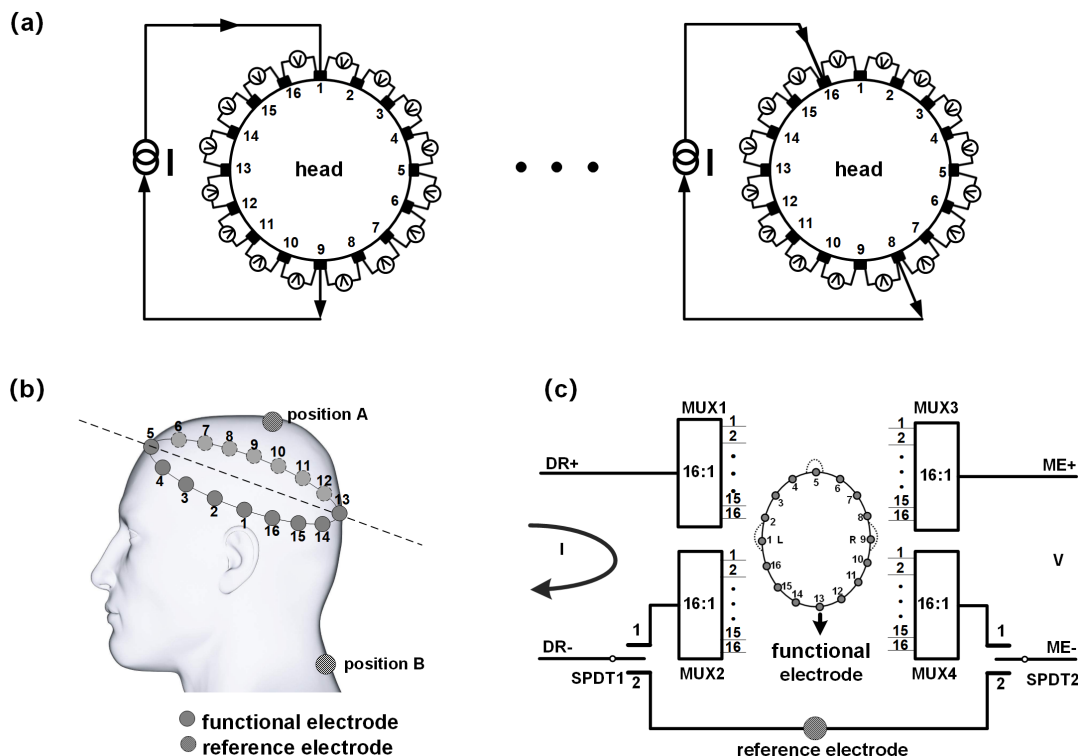


FIGURE 1. Diagrams of the experimental setup in this study. (a) Data acquisition using EIT system by exciting pairs of opposite electrodes and measuring pairs of adjacent electrodes. (b) Functional and reference electrodes attached to the volunteer’s scalp. (c) Control circuit for the electrode channels of the EIT system. The circuit comprises four 16:1 multiplexers (MUX1 to MUX4) and two single-pole double-throw switches (SPDT1 and SPDT2).

Boone *et al.* [28] developed an electrical circuit model to assess the effect of the contact impedances of multiple electrode–skin interfaces on signal acquisition and image reconstruction of EIT. They found that 1) a 2% change in the contact impedance notably distorts the detected signal, 2) a 5% change almost vanishes the target signal, and 3) a change of 10% or above results in false features appearing in the reconstructed images. Nevertheless, the improved performance of currently available electronic components may further reduce the impact of multi-channel contact impedances on the EIT performance.

On the other hand, the effect of contact impedance on the output of the current source has not been considered. Using the finite element method, Boyle *et al.* [29] found that, when the variation in the multi-channel contact impedances is above 20%, the reconstructed image contains considerable artifacts, thus biasing clinical diagnostics. However, their study was based on a simplified two-dimensional model, and the parameters of contact impedance neglected the characteristics of multi-channel contact impedances in clinical environments. Moreover, the impact of multi-channel contact impedances on the output of the excitation current source and the accuracy of signal acquisition were not considered.

Traditional techniques for bioelectrical signal detection (e.g., electroencephalography and electrocardiography) are also affected by the electrode–skin contact impedances, but at a much lower extent than in EIT. In fact, the signal frequency in traditional bioelectrical signal detection is much lower

than the working frequency of EIT, which is usually between several and hundreds of kilohertz [30], and electrodes in traditional techniques are only used for passive signal detection. Furthermore, cerebral time-difference EIT is even more sensitive to the change over time in multi-channel contact impedances.

In this study, we developed a method based on a common reference electrode for real-time monitoring of multi-channel contact impedances during cerebral EIT. This method—implemented on an existing cerebral EIT system—allows to capture inter-channel differences and change over time of multi-channel contact impedances. We experimentally verified the proposed method by systematically monitoring the distribution and variation of the multi-channel contact impedances of the EIT system during brain imaging of volunteers. The data of multi-channel contact impedances obtained from the experiments were used for a preliminary analysis regarding the effect of multi-channel contact impedances on signal detection.

The remainder of this paper is organized as follows. In Section II, the operation of the time-difference EIT system and the method for monitoring multi-channel contact impedances are presented. Section III describes the system experiments with the participation of human subjects. In Section IV, the experimental results are analyzed to demonstrate the characteristics of multi-channel contact impedances during EIT imaging. Finally, we draw conclusions in Section V and outline suggestions for future research.

II. METHODS

A. OPERATION OF TIME-DIFFERENCE EIT

The EIT system considered in this study is equipped with 16 electrodes, which are evenly distributed along a transverse cross-section of the human head. The system collects data by injecting excitation currents to pairs of opposite electrodes and measuring signals at pairs of adjacent electrodes, as shown in Fig. 1(a). For data acquisition, an excitation current is injected into the human body through the first pair of opposite electrodes (1–9). The current is designed according to standard IEC 60601-1 [31] to guarantee safe ranges for frequency and amplitude. During excitation current injection, the system sequentially measures the voltages of the 16 pairs of adjacent electrodes (1–2, 2–3, ..., 16–1). Then, the system sequentially switches the excitation current to the other 15 pairs of opposite electrodes (2–10, 3–11, ..., 16–8), and again sequentially measures the voltages of the 16 pairs of adjacent electrodes per pair of excitation electrodes. This measurement process generates $16 \times 16 = 256$ voltage measurements, which compose a data frame. Time-difference EIT uses two data frames obtained at two different times to reconstruct the distribution of electrical impedance variation over the target area.

B. REFERENCE ELECTRODE METHOD

Although noninvasive methods for accurate measurement of contact impedance are not available, common methods for indirect estimation of contact impedance include the two-electrode method [32], [33] and reconstruction method [34]–[36]. The two-electrode method yields the sum of the contact impedances of two electrode–skin interfaces, and thus cannot provide the contact impedance of any individual interface. Usually, the two-electrode method has been used to evaluate the performance of electrode materials.

We propose the use of a reference electrode method for real-time monitoring of the 16-channel contact impedances from the EIT system. The method works by adding a reference electrode to the existing array of 16 electrodes. Hereafter, the 16 electrodes for imaging are called functional electrodes to distinguish them from the reference electrode. The reference electrode is attached to either the top of the head (position A in Fig. 1(b)) or the back of the neck (position B in Fig. 1(b)). Only when the top of the head does not satisfy the conditions required by placing the reference electrode, it is attached to the back of the neck. The 16 functional electrode channels are controlled using four 16:1 multiplexers (MUX1 to MUX4), as shown in Fig. 1(c), to realize any combination required for boundary voltage measurement. The reference electrode channel is controlled using two analog single-pole double-throw switches (SPDT1 and SPDT2) for the system to be switched between the modes of boundary voltage and contact impedance measurements. The reference electrode method comprises two steps and uses the measurement principle illustrated in Fig. 2(a).

Step 1: First, the two-electrode method is used to measure the impedances of each pair of adjacent functional electrodes and the impedance between the first and third functional electrodes. Thereby, initial estimates of the 16-channel contact impedances and their differences can be obtained. This step proceeds as follows. Switches SPDT1 and SPDT2 are connected to contact 1. Hence, electrodes E_m and E_p are the same, as well as E_n and E_q . Then, the impedance is measured between E_m and E_n using the two-electrode method. The measured impedance ($Z_{m,n}$) is the sum of the contact impedances of E_m and E_n (Z_{c_m} and Z_{c_n} , respectively). As the transfer impedance between the two electrodes ($Z_{t_{m,n}}$) is much smaller than Z_{c_m} and Z_{c_n} , $Z_{m,n}$ is usually taken as approximately equal to the sum of Z_{c_m} and Z_{c_n} . The other 16 pairs of adjacent electrodes are then measured using the same approach. Then, the impedance between E_1 and E_3 is measured using the two-electrode method. Finally, the contact impedances of the 16 electrodes are estimated as

$$Z_c = M^{-1} \cdot Z_m \tag{1}$$

where Z_c is the column vector of contact impedances of the 16 electrodes, Z_m is the column vector of the 17 measurements, and M is a coefficient matrix:

$$M = \begin{bmatrix} 1 & 1 & 0 & \dots & 0 & 0 \\ 0 & 1 & 1 & & 0 & 0 \\ & \vdots & & \ddots & & \vdots \\ 1 & 0 & 0 & \dots & 0 & 1 \\ 1 & 0 & 1 & & 0 & 0 \end{bmatrix}$$

$$Z_c = \begin{bmatrix} Z_{c_1} \\ Z_{c_2} \\ \vdots \\ Z_{c_{16}} \end{bmatrix}, \quad Z_m = \begin{bmatrix} Z_{m_1} \\ Z_{m_2} \\ \vdots \\ Z_{m_{17}} \end{bmatrix} \tag{2}$$

Step 2: During the interval of two adjacent frames of boundary voltage measurements, the impedances between every functional electrode and the reference electrode are sequentially measured using the two-electrode method. This way, the change over time of the impedances at the 16 channels can be obtained as follows. Switches SPDT1 and SPDT2 are connected to contact 1 to enter the mode of boundary voltage measurement. Here, E_m , E_p , E_n , and E_q correspond to any four of the 16 functional electrodes, and the combination is controlled through multiplexers MUX1 to MUX4. From the four electrodes, E_m and E_n are the pair of excitation electrodes, and E_p and E_q are the pair of measurement electrodes. After completing a frame of boundary voltage measurements, SPDT1 and SPDT2 are simultaneously switched to contact 2 to enter the mode of contact impedance measurement. Then, E_m and E_p are set as the same functional electrode by controlling MUX1 and MUX3, and the impedance between E_m and E_{ref} is measured using the two-electrode method. The impedances between the other 15 functional electrodes and the reference electrode are measured using the same approach. Then, SPDT1 and SPDT2 are

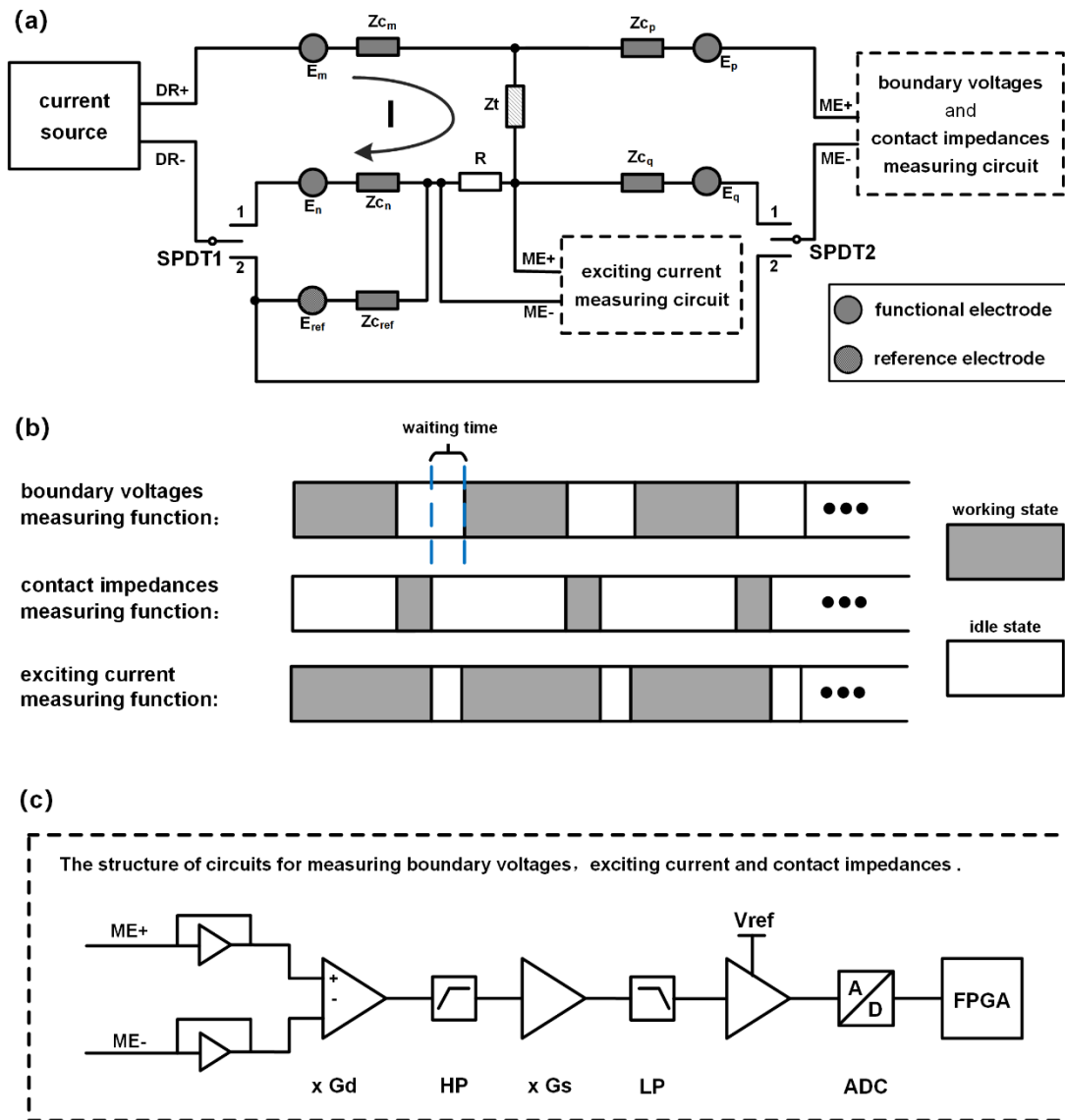


FIGURE 2. Proposed reference electrode method. (a) Measurement principle of reference electrode method. When SPDT1 and SPDT2 are simultaneously connected to contact 1, the system switches to the mode of boundary voltage measurement, in which functional electrodes m and n serve as the pair of excitation electrodes and functional electrodes p and q serve as the pair of measurement electrodes. When SPDT1 and SPDT2 are simultaneously connected to contact 2, the system switches to the mode of contact impedance measurement, in which functional electrode m and the reference electrode serve as both the pair of excitation electrodes and the pair of measurement electrodes. (b) Time sequence for measuring boundary voltage, contact impedance, and excitation current. (c) Block diagram of signal acquisition circuit consisting of buffer amplifiers, differential amplifier $\times G_d$, high-pass (HP) filter, downstream single-end amplifier $\times G_s$, low-pass (LP) filter, voltage level lifting circuit, and an analog-to-digital converter (ADC).

connected to contact 1 to restore the mode of boundary voltage measurement.

As shown in Fig. 2(a), $Z_{m,ref}$ is the sum of the impedance across the tissue between the m -th functional electrode and the reference electrode ($Z_{t,m,ref}$), the sampling resistance (R), the contact impedance of the reference electrode ($Z_{C_{ref}}$), and the contact impedance of the m -th functional electrode (Z_{C_m}):

$$Z_{m,ref} = Z_{t,m,ref} + R + Z_{C_{ref}} + Z_{C_m} \quad (3)$$

where $m = 1, 2, \dots, 16$, and $Z_{t,m,ref} \ll Z_{C_m}$. The reference electrode should be larger than the functional electrode to

ensure $Z_{C_{ref}} \ll Z_{C_m}$. As the value of R is known, $Z_{m,ref}$ is substituted by $(Z_{m,ref} - R)$ hereafter.

Fig. 2(b) shows the time sequence of the three modes of measurement, namely, boundary voltage, contact impedance, and excitation current. The system alternates between the two modes of boundary voltage and contact impedance measurement. To reduce the hardware size, the two modes of measurement were designed to share the same signal acquisition circuit. The mode of excitation current measurement was designed for real-time monitoring the output of the excitation current source and computing the contact impedance. In addition, it runs parallel to the other two modes by being

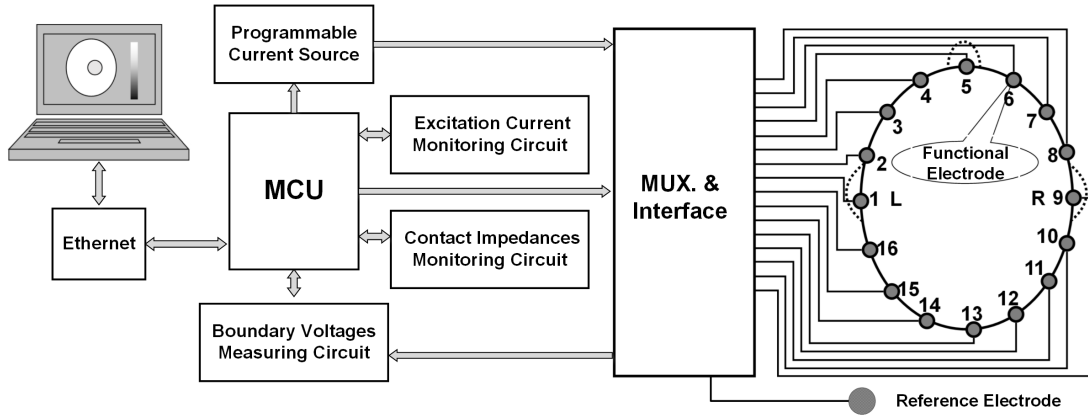


FIGURE 3. Block diagram of EIT system. (MCU, multipoint control unit).

implemented on a separate signal acquisition circuit. Each of the two signal acquisition circuits consists of buffer amplifiers, an upstream program-controlled differential amplifier ($\times G_d$), a high-pass filter, a downstream program-controlled single-end amplifier ($\times G_s$), a low-pass filter, a voltage level lifting circuit, and an analog-to-digital converter, as shown in Fig. 2(c).

The proposed reference electrode method was realized by adjusting the circuit of the high-precision EIT data acquisition system for brain imaging introduced in [37]. We used a modular design and incorporated a reference electrode control module into the multiplexer and interface subsystem. Fig. 3 shows the block diagram of the resulting hardware system. It satisfies the requirements for high-precision brain imaging as verified experimentally.

C. ANALYSIS OF MULTI-CHANNEL CONTACT IMPEDANCES

Let $\Delta Z_m(t_0, t)$ be defined as

$$\begin{aligned} \Delta Z_m(t_0, t) &= Z_{m,ref}(t) - Z_{m,ref}(t_0) \\ &= \{Z_{t_{m,ref}}(t) - Z_{t_{m,ref}}(t_0)\} \\ &\quad + \{Z_{C_{ref}}(t) - Z_{C_{ref}}(t_0)\} + \{Z_{C_m}(t) - Z_{C_m}(t_0)\} \\ &= \Delta Z_{t_{m,ref}}(t_0, t) + \Delta Z_{C_{ref}}(t_0, t) + \Delta Z_{C_m}(t_0, t) \end{aligned} \quad (4)$$

where $\Delta Z_{t_{m,ref}}(t_0, t)$ is the variation in impedance of the tissue between the m -th functional electrode and the reference electrode during time interval $t_0 - t$, $\Delta Z_{C_{ref}}(t_0, t)$ is the variation in the contact impedance of the reference electrode, and $\Delta Z_{C_m}(t_0, t)$ is the variation in the contact impedance of the m -th functional electrode, both during time interval $t_0 - t$.

Given that $Z_{t_{m,ref}} \ll Z_{C_m}$, $Z_{C_{ref}} \ll Z_{C_m}$, and Z_{C_m} is more prone to variation by external factors, we proved that $\Delta Z_{t_{m,ref}}(t_0, t) \ll \Delta Z_{C_m}(t_0, t)$ and $\Delta Z_{C_{ref}}(t_0, t) \ll \Delta Z_{C_m}(t_0, t)$ through preliminary experiments. Thus,

$$\Delta Z_m(t_0, t) = Z_{m,ref}(t) - Z_{m,ref}(t_0) \approx \Delta Z_{C_m}(t_0, t) \quad (5)$$

The contact impedances of the 16 channels at time t_0 , $Z_{C_m}(t_0)$, which we use as base values of the contact impedances for

subsequent analyses, can be estimated using (1), and the contact impedances at time t , $Z_{C_m}(t)$, can be computed as

$$\begin{aligned} Z_{C_m}(t) &= Z_{C_m}(t_0) + \Delta Z_{C_m}(t_0, t) \\ &= Z_{C_m}(t_0) + \{Z_{m,ref}(t) - Z_{m,ref}(t_0)\} \\ &= Z_{C_m}(t_0) + \Delta Z_m(t_0, t) \end{aligned} \quad (6)$$

Then, the difference between the contact impedances of the m -th and n -th channels ($Z_{C_m}(t)$ and $Z_{C_n}(t)$, respectively) can be expressed as

$$\begin{aligned} \Delta Z_{C_{m,n}}(t) &= Z_{C_m}(t) - Z_{C_n}(t) \\ &= \{Z_{C_m}(t_0) + \Delta Z_m(t_0, t)\} - \{Z_{C_n}(t_0) + \Delta Z_n(t_0, t)\} \\ &= \{Z_{C_m}(t_0) - Z_{C_n}(t_0)\} + \{\Delta Z_m(t_0, t) - \Delta Z_n(t_0, t)\} \end{aligned} \quad (7)$$

where $\Delta Z_m(t_0, t)$ and $\Delta Z_n(t_0, t)$ can be obtained from (5).

Then, the mean contact impedance of each channel (\bar{Z}_{C_m}) can be computed using (8). In addition, the maximum relative variation of the contact impedance per channel (δ_m) can be obtained using (9), and the maximum variation of the contact impedances from the 16 channels, δ , which characterizes the change over time in the contact impedances from all the channels, can be obtained using (10). Furthermore, the maximum difference between contact impedances of the 16 channels, γ , which characterizes the differences between the contact impedances of the channels, can be obtained using (11), where $m, n = 1, 2, \dots, 16$.

$$\bar{Z}_{C_m} = \sum_{k=1}^{7200} Z_{C_m}(t_k) / 7200 \quad (8)$$

$$\begin{aligned} \delta_m &= \frac{\Delta Z_{C_m}}{\bar{Z}_{C_m}} \\ &= \frac{\max_{k=1}^{7200} \{Z_{C_m}(t_k)\} - \min_{k=1}^{7200} \{Z_{C_m}(t_k)\}}{\bar{Z}_{C_m}} \end{aligned} \quad (9)$$

$$\delta = \max_{m=1}^{16} \{\delta_m\} \quad (10)$$

$$\gamma = \max_{k=1}^{7200} \left\{ \frac{\max_{m,n=1}^{16} \{\Delta Z_{C_{m,n}}(t_k)\}}{\min_{m=1}^{16} \{Z_{C_m}(t_k)\}} \right\} \quad (11)$$

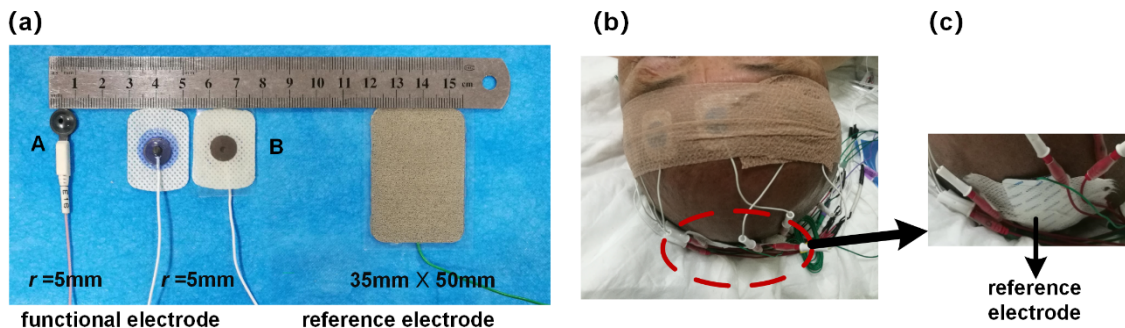


FIGURE 4. Photographs of experimental equipment and setup. (a) Functional electrodes (Ag/AgCl powder electrode (type A) and disposable surface electrode (type B)) and reference electrode. (b) Functional electrodes attached to the head of a volunteer. (c) Reference electrode attached at the top of the head of a volunteer.

III. EXPERIMENTS

We considered the cerebral EIT system as experimental platform to evaluate the proposed method. The method can monitor in real time the contact impedances of the 16 EIT channels, as shown in Fig. 1(b). Two types of functional electrodes were used for the experiment, namely, Ag/AgCl powder electrodes (Oxford Instruments, Abingdon, UK) and disposable surface electrodes (Friendship Medical Electronics Company Ltd, Xi'an, China). Fig. 4(a) shows photos and indicates the geometrical dimensions of the two types of functional electrodes and the reference electrode. The functional electrode region to be in contact with the human body is made from Ag/AgCl, has a small polarization potential and 10 mm in diameter. The reference electrode is a disposable grounded electrode for medical applications (Friendship Medical Electronics Company Ltd), has an effective area of skin contact of 35×50 mm, is manufactured from Ag/AgCl, is self-adhesive, and can remain in contact with the skin for long periods.

Thirty-six healthy male volunteers with ages of 39 ± 17 years were recruited for the experiment. They neither had cerebrovascular disease nor experienced any traumatic brain injury. The 36 volunteers were randomly divided into two groups of 18 participants each. The Ag/AgCl powder electrodes were used for group 1 and attached to the skin using a conductive paste (Elefix, Z-410CE; Nihon Kohden, Tokyo, Japan). The disposable surface electrodes were used for group 2 and attached to the skin using hydrogel. The same type of reference electrode was used for both groups. This study was approved by the Fourth Military Medical University Ethics Committee of Human Research, and informed written consent was obtained from all the volunteers.

To prepare for the experiment, the head hairs of the volunteers were removed, and their scalps were cleaned. Sixteen functional electrodes were attached to the head of each volunteer and numbered as shown in Fig. 1(b). Fig. 4(b) shows a photograph of the electrode arrangement on a volunteer. The reference electrode was attached to the top of the volunteer's head, as shown in Fig. 4(c). After the electrodes were attached, the volunteer laid on his back on a bed during the measurements. Meanwhile, the EIT system was initialized and allowed to warm up for 30 min, with excitation

current of 1.25 mA_{p-p} and frequency of 50 kHz. All the volunteers were tested in the same laboratory room, which was well insulated and had environmental temperature of 26.0 ± 2.0 °C and relative humidity of $35 \pm 10\%$.

Each volunteer was continuously monitored for 2 h. A data frame of boundary voltage measurements and a frame of contact impedance measurements were collected every second. During the test, the volunteer remained comfortable and was asked to be relaxed. The body movements of the volunteer were also recorded. After completing the test, the electrodes were removed from the volunteer, and his scalp was cleaned.

IV. RESULTS AND ANALYSIS

A. MONITORING RESULTS OVER 2 HOURS IN PRELIMINARY EXPERIMENT

Fig. 5(a) shows the estimates of real-time contact impedances $Z_{c_m}(t)$ at the 16 channels obtained from the 2-hour EIT test of one volunteer in group 1 (i.e., using electrode type A). The contact impedance of the 13th channel at 3600 s notably deviates, and that of the 12th channel slightly deviates. The record shows that the volunteer made substantial body movements during this part of the experiment. Fig. 5(b) shows the real-time monitoring results for one volunteer in group 2 (i.e., using electrode type B). Unlike the other channels, the contact impedance of the 13th channel exhibits remarkable temporal fluctuations.

Figs. 5(c) and 5(d) present the average, maximum, and minimum values of the contact impedances in Figs. 5(a) and 5(b), respectively. The contact impedances measured using electrode type A have a smaller mean value but larger inter-channel differences and change over time than those measured using electrode type B.

This may be explained by the different conductive agents used at the electrode–skin interface. In fact, electrode type B was supplied with a layer of hydrogel, which serves as agent to bound the electrode to the skin and conductive medium at the electrode–skin interface, whereas electrode type A was attached to the skin by applying a layer of conductive paste at the electrode–skin interface. As the conductivity of the hydrogel is poorer than that of the conductive paste, the contact impedance of electrode type B is higher than that

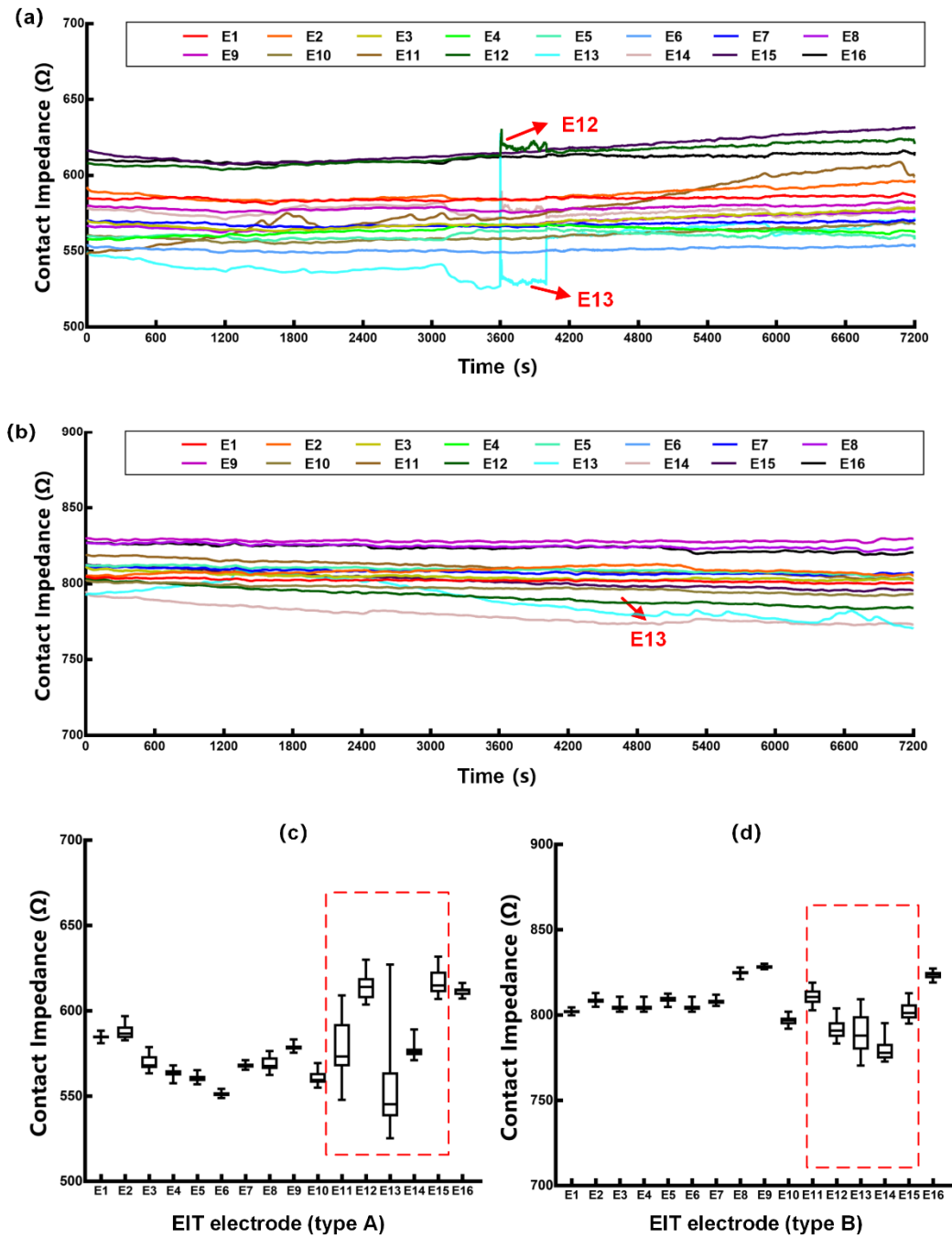


FIGURE 5. Monitoring results. (a) Continuously monitored contact impedances of the electrode type A during the preliminary experiment for 2h. (b) Continuously monitored contact impedances of the electrode type B during the preliminary experiment for 2h. Statistical results of (c) data shown in Fig. 5(a) and (d) data shown in Fig. 5(b) (mean, maximum, and minimum values).

of electrode type A. On the other hand, the layer of hydrogel is uniform in thickness and shape, unlike the conductive paste. Hence, the contact impedances measured using electrode type A exhibited larger inter-channel differences (lower spatial consistency) than those measured using electrode type B. Furthermore, hydrogel has a better moisture-holding capacity than conductive paste. In other words, the effectiveness of

the conductive paste decreases more notably with time than that of the hydrogel. Consequently, the contact impedances measured using electrode type A show larger changes over time.

Overall, the contact impedances of the EIT system measured using electrode type A have larger inter-channel differences and change over time than those measured

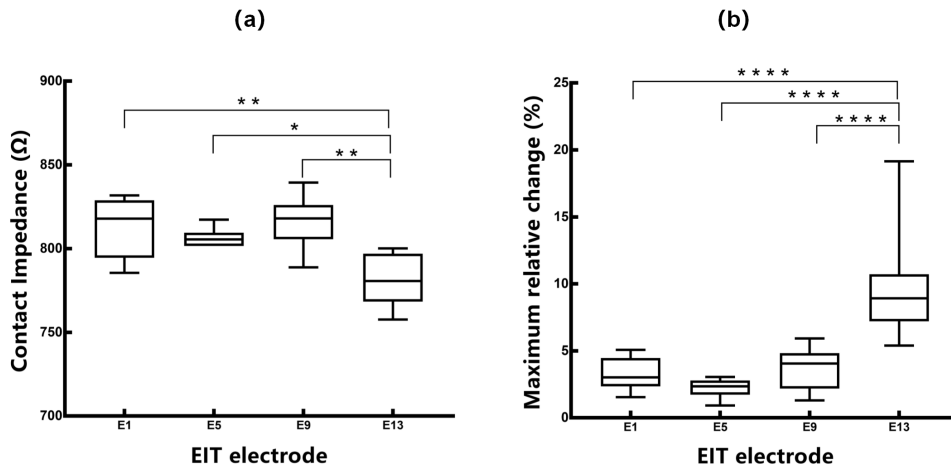


FIGURE 6. Statistical analysis results of contact impedances measured at four different parts of the human head ($N = 18$). (a) Mean value of contact impedance and (b) maximum relative change over time of contact impedance. (*: $p < 0.05$; **: $p < 0.01$; ****: $p < 0.0001$).

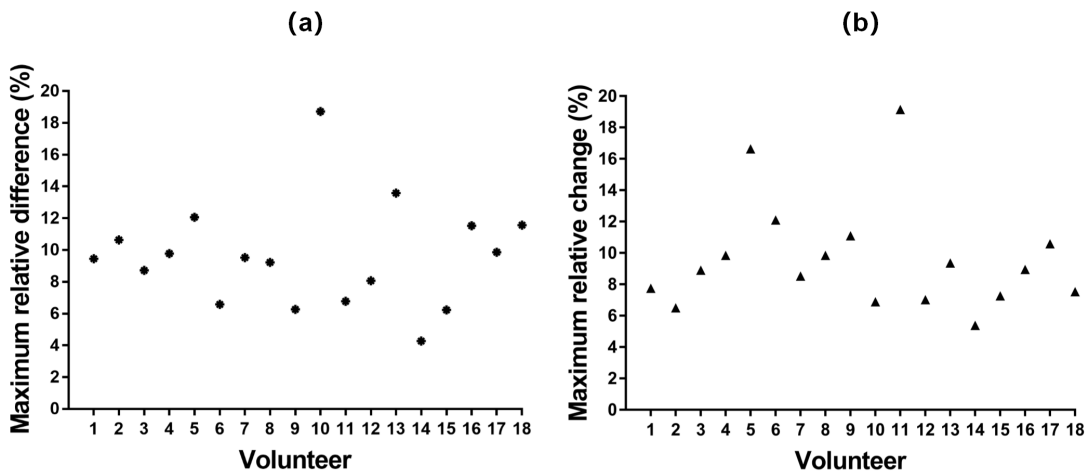


FIGURE 7. Statistical analysis results of contact impedances from the 18 volunteers in group 2 (measured using disposable surface electrodes) ($N = 18$). (a) Maximum relative difference between contact impedances (γ) and (b) maximum relative change over time of the contact impedances (δ) at the 16 channels.

using electrode type B. Therefore, the multi-channel contact impedances of the EIT system measured using electrode type B were used for subsequent analyses.

B. COMPARISON OF CONTACT IMPEDANCES AT FOUR POSITIONS

To investigate the effect of the electrode location on the contact impedance, we performed a one-way ANOVA analysis ($N = 18$) to the contact impedances measured at the following four electrodes: E_1 (above the left ear), E_5 (at the center of the forehead), E_9 (above the right ear), and E_{13} (at the occiput). Fig. 6(a) shows the mean values of the contact impedances at these four electrodes. The mean contact impedance at E_{13} is significantly ($p < 0.05$) lower than that at the other three electrodes, E_1 , E_5 , and E_9 , by 8.7, 6.9, and 8.6%, respectively. The differences between the contact impedances at E_1 , E_5 , and E_9 are not statistically significant. Fig. 6(b) shows the statistical analysis results of the change over time in the

contact impedances at the four electrodes. The change of contact impedance over time at E_{13} is significantly ($p < 0.05$) higher than that at the other three electrodes, E_1 , E_5 , and E_9 .

This trend may be explained by the fact that the volunteer laid down on his back during the experiment. When the volunteer maintained this posture, the electrodes at the occiput were squeezed against the scalp and showed improved contact with the skin, thus reducing the contact impedance measurements. When the volunteer moved his head, the contact between the electrode fixed at the occiput and his skin was more prone to variation, thus resulting in higher change over time in the contact impedances measured at this electrode. Furthermore, some volunteers had a scalp with slackness, and the friction between the bolster and scalp possibly resulted in shifts of the scalp and consequent shifts of the electrode attached at the occiput. Therefore, higher change over time occurred in the contact impedances measured at this electrode.

TABLE 1. Statistical results of contact impedances at the 16 channels (N = 18).

Characteristic	Maximum (%)	Minimum (%)	Mean (%)
Relative inter-channel difference (γ)	18.7	4.3	9.5
Relative variation within 2 hours (δ)	19.2	5.4	9.7

C. CHARACTERISTICS OF 16-CHANNEL CONTACT IMPEDANCES

The relative difference between the contact impedances of the 16 channels (γ) and their relative change over time (δ) were computed using (10) and (11), respectively, obtaining the results shown in Figs. 7(a) and 7(b), respectively. Table 1 lists the statistical results of the multi-channel contact impedances of the 18 volunteers in group 2 (i.e., using electrode type B). Under this more ideal testing condition (compared to the use of electrode type A), the contact impedances of the 16 channels of the EIT have mean, maximum, and minimum inter-channel differences of 9.5, 18.7, and 4.3%, respectively, and mean, maximum, and minimum change over time of 9.7, 19.2, and 5.4%, respectively, as shown in Table 1.

V. CONCLUSION

We propose a reference-electrode method to monitor in real time the multi-channel contact impedances of cerebral EIT. The method comprises two steps: 1) when the EIT system is initialized, the multi-channel contact impedances are estimated as basis for subsequent monitoring; 2) in the intervals of boundary voltage measurements, real-time monitoring of change over time of the multi-channel impedances is conducted. Hence, the proposed method offers real-time evaluation of the spatial distribution differences and change over time of multi-channel impedances. Although the method cannot accurately measure the true values of multi-channel impedances, it presents the following advantages: 1) at monitoring onset, a quick estimation of the multi-channel impedances can be used as basis for subsequent analyses and reference for attaching the electrodes; 2) the multi-channel contact impedances can be quickly obtained, in tens of milliseconds, after measuring the boundary voltages. Therefore, we consider feasible to track the change of contact impedances over time during boundary voltage measurements in real time with few electrode channel switches and without affecting the measurements.

We verified the proposed method during EIT measurements on several volunteers. The contact impedances of EIT measured using the disposable surface electrodes have smaller inter-channel differences and change over time than those measured using the Ag/AgCl powder electrodes. The contact impedances of the 16 channels of the cerebral EIT system using the disposable surface electrodes have maximum relative inter-channel difference of 18.7% and maximum relative change over time of 19.2%.

Under the more ideal testing condition (i.e., using the disposable surface electrodes providing better contact impedance for long-time monitoring), the effects of both the difference between contact impedances and their change over time at the 16 channels are dependent on image reconstruction. For clinical application of EIT, where the testing environments may be more intricate than the laboratory environment in this study, these effects on signal detection and image reconstruction of EIT may be even more considerable.

There are at least two ways to use the data obtained from the proposed reference-electrode method in practice. First, it can flag poor electrode contact and corrupted data, as contact impedances directly reflect the contact quality of electrodes with the scalp, which in turn affects data acquisition. Second, data may be used for correcting measured voltages and improving image reconstruction.

ACKNOWLEDGMENT

(Hang Ma and Haoting Li contributed equally to this work.)

REFERENCES

- [1] D. C. Barber, B. H. Brown, and I. L. Freeston, "Imaging spatial distributions of resistivity using applied potential tomography," *Electron. Lett.*, vol. 19, no. 2, pp. 933–935, Oct. 1983.
- [2] D. S. Holder and A. R. Gardner-Medwin, "Some possible neurological applications of applied potential tomography," *Clin. Phys. Physiol. Meas.*, vol. 9, pp. 111–119, Jan. 1988.
- [3] D. S. Holder, "Electrical impedance tomography: Methods, history and applications," *Med. Phys.*, vol. 32, no. 8, p. 2731, 2005.
- [4] R. Bayford and A. Tizzard, "Bioimpedance imaging: An overview of potential clinical applications," *Analyst*, vol. 137, no. 20, pp. 4635–4643, Oct. 2012.
- [5] R. J. Sadleir, T. Tang, A. S. Tucker, P. Borum, and M. Weiss, "Detection of intraventricular blood using EIT in a neonatal piglet model," in *Proc. Annu. Int. Conf. IEEE Eng. Med. Biol. Soc.*, Sep. 2009, pp. 3169–3172.
- [6] J. P. Morucci and B. Rigaud, "Bioelectrical impedance techniques in medicine. Part III: Impedance imaging. Third section: Medical applications," *Crit. Rev. Biomed. Eng.*, vol. 24, nos. 4–6, pp. 655–677, Jan. 1996.
- [7] M. T. Clay and T. C. Ferree, "Weighted regularization in electrical impedance tomography with applications to acute cerebral stroke," *IEEE Trans. Med. Imag.*, vol. 21, no. 6, pp. 629–637, Jun. 2002.
- [8] S. Wanjuan, Y. Fusheng, Z. Wei, Z. Hongyi, F. Feng, S. Xuetao, L. Ruigang, X. Canhua, D. Xiuzhen, and B. Tingyi, "Image monitoring for an intraperitoneal bleeding model of pigs using electrical impedance tomography," *Physiol. Meas.*, vol. 29, no. 2, pp. 217–225, Feb. 2008.
- [9] W. Shuai, F. You, H. Zhang, W. Zhang, F. Fu, X. Shi, R. Liu, T. Bao, and X. Dong, "Application of electrical impedance tomography for continuous monitoring of retroperitoneal bleeding after blunt trauma," *Ann. Biomed. Eng.*, vol. 37, no. 11, pp. 2373–2379, Nov. 2009.
- [10] C. H. Xu, L. Wang, X. T. Shi, F. S. You, F. Fu, R. G. Liu, M. Dai, Z. W. Zhao, G. D. Gao, and X. Z. Dong, "Real-time imaging and detection of intracranial haemorrhage by electrical impedance tomography in a piglet model," *J. Int. Med. Res.*, vol. 38, no. 5, pp. 1596–1604, Oct. 2010.
- [11] T. Tang, S. Oh, and R. J. Sadleir, "A robust current pattern for the detection of intraventricular hemorrhage in neonates using electrical impedance tomography," *Ann. Biomed. Eng.*, vol. 38, no. 8, pp. 2733–2747, Aug. 2010.
- [12] M. Dai, L. Wang, C. Xu, L. Li, G. Gao, and X. Dong, "Real-time imaging of subarachnoid hemorrhage in piglets with electrical impedance tomography," *Physiol. Meas.*, vol. 31, no. 9, pp. 1229–1239, Sep. 2010.
- [13] T. Tang, M. D. Weiss, P. Borum, S. Turovets, D. Tucker, and R. Sadleir, "In vivo quantification of intraventricular hemorrhage in a neonatal piglet model using an EEG-layout based electrical impedance tomography array," *Physiol. Meas.*, vol. 37, no. 6, pp. 751–764, Jun. 2016.

- [14] G. Boverman, T. J. Kao, X. Wang, J. M. Ashe, D. M. Davenport, and B. C. Amm, "Detection of small bleeds in the brain with electrical impedance tomography," *Physiol. Meas.*, vol. 37, no. 6, pp. 727–753, Jun. 2016.
- [15] O. Casas, R. Bragós, P. J. Riu, J. Rosell, M. Tresànceh, M. Warren, A. Rodríguez-Sinovas, A. Carreño, and J. Cinca, "In vivo and in situ ischemic tissue characterization using electrical impedance spectroscopy," *Ann. New York Acad. Sci.*, vol. 873, no. 1, pp. 51–58, Apr. 1999.
- [16] N. Goren, J. Avery, T. Dowrick, E. Mackle, A. Witkowska-Wrobel, D. Werring, and D. Holder, "Multi-frequency electrical impedance tomography and neuroimaging data in stroke patients," *Sci. Data*, vol. 5, Jul. 2018, Art. no. 180112.
- [17] A. Romsauerova, A. McEwan, L. Horesh, R. Yerworth, R. H. Bayford, and D. S. Holder, "Multi-frequency electrical impedance tomography (EIT) of the adult human head: Initial findings in brain tumours, arteriovenous malformations and chronic stroke, development of an analysis method and calibration," *Physiol. Meas.*, vol. 27, p. S147–S161, May 2006.
- [18] J. Avery, T. Dowrick, M. Faulkner, N. Goren, and D. Holder, "A versatile and reproducible multi-frequency electrical impedance tomography system," *Sensors*, vol. 17, no. 2, p. E280, Jan. 2017.
- [19] Y. Li, D. Zhang, B. Liu, Z. Jin, W. Duan, X. Dong, F. Fu, S. Yu, and X. Shi, "Noninvasive cerebral imaging and monitoring using electrical impedance tomography during total aortic arch replacement," *J. Cardiothoracic Vascular Anesthesia*, vol. 32, no. 6, pp. 2469–2476, Dec. 2018.
- [20] P. K. Manwaring, K. L. Moodie, A. Hartov, K. H. Manwaring, and R. J. Halter, "Intracranial electrical impedance tomography: A method of continuous monitoring in an animal model of head trauma," *Anesthesia Analgesia*, vol. 117, no. 4, pp. 866–875, Oct. 2013.
- [21] M. Soleimani, C. Gómezlaberge, and A. Adler, "Imaging of conductivity changes and electrode movement in EIT," *Physiol. Meas.*, vol. 27, no. 5, p. S103, Apr. 2006.
- [22] A. E. Hartinger, H. Gagnon, and R. Guardo, "Accounting for hardware imperfections in EIT image reconstruction algorithms," *Physiol. Meas.*, vol. 28, no. 7, pp. S13–S27, Jul. 2007.
- [23] A. E. Hartinger, R. Guardo, A. Adler, and H. Gagnon, "Real-time management of faulty electrodes in electrical impedance tomography," *IEEE Trans. Biomed. Eng.*, vol. 56, no. 2, pp. 369–377, Feb. 2009.
- [24] A. Adler, "Accounting for erroneous electrode data in electrical impedance tomography," *Physiol. Meas.*, vol. 25, no. 1, pp. 227–238, Feb. 2004.
- [25] R. Cardu, P. H. Leong, C. T. Jin, and A. McEwan, "Electrode contact impedance sensitivity to variations in geometry," *Physiol. Meas.*, vol. 33, no. 5, pp. 817–830, May 2012.
- [26] X. Liu, J. Yao, T. Zhao, H. Obara, Y. Cui, and M. Takei, "Image reconstruction under contact impedance effect in micro electrical impedance tomography sensors," *IEEE Trans. Biomed. Circuits Syst.*, vol. 12, no. 3, pp. 623–631, Jun. 2018.
- [27] M. Guermandi, R. Cardu, E. F. Scarselli, and R. Guerrieri, "Active electrode IC for EEG and electrical impedance tomography with continuous monitoring of contact impedance," *IEEE Trans. Biomed. Circuits Syst.*, vol. 9, no. 1, pp. 21–33, Feb. 2015.
- [28] K. G. Boone and D. S. Holder, "Effect of skin impedance on image quality and variability in electrical impedance tomography: A model study," *Med. Biol. Eng. Comput.*, vol. 34, no. 5, pp. 351–354, Sep. 1996.
- [29] A. Boyle and A. Adler, "The impact of electrode area, contact impedance and boundary shape on EIT images," *Physiol. Meas.*, vol. 32, no. 7, pp. 745–754, Jul. 2011.
- [30] L. Yang, M. Dai, C. Xu, G. Zhang, W. Li, F. Fu, X. Shi, and X. Dong, "The frequency spectral properties of electrode-skin contact impedance on human head and its frequency-dependent effects on frequency-difference eit in stroke detection from 10 Hz to 1 MHz," *PLoS ONE*, vol. 12, no. 1, Jan. 2017, Art. no. e0170563.
- [31] *Medical Electrical Equipment Part 1: General Requirements for Basic Safety and Essential Performance*, Standard I. 60601-1:2015, International Electrotechnical Commission, 2015.
- [32] S. Xu, M. Dai, C. Xu, C. Chen, M. Tang, X. Shi, and X. Dong, "Performance evaluation of five types of Ag/AgCl bio-electrodes for cerebral electrical impedance tomography," *Ann. Biomed. Eng.*, vol. 39, no. 7, pp. 2059–2067, Jul. 2011.
- [33] L. Yang, H. Li, J. Ding, W. Li, X. Dong, Z. Wen, and X. Shi, "Optimal combination of electrodes and conductive gels for brain electrical impedance tomography," *Biomed. Eng. Online*, vol. 17, no. 1, p. 186, Dec. 2018.
- [34] A. Nissinen, L. M. Heikkinen, V. Kolehmainen, and J. P. Kaipio, "Compensation of errors due to discretization, domain truncation and unknown contact impedances in electrical impedance tomography," *Meas. Sci. Technol.*, vol. 20, no. 10, Oct. 2009, Art. no. 105504.
- [35] A. Nissinen, J. P. Kaipio, M. Vauhkonen, and V. Kolehmainen, "Contrast enhancement in EIT imaging of the brain," *Physiol. Meas.*, vol. 37, no. 1, pp. 1–24, Dec. 2016.
- [36] L. M. Heikkinen, T. Vilhunen, R. M. West, and M. Vauhkonen, "Simultaneous reconstruction of electrode contact impedances and internal electrical properties: II. Laboratory experiments," *Meas. Sci. Technol.*, vol. 13, no. 12, pp. 1848–1854, Nov. 2002.
- [37] X. Shi, W. Li, F. You, X. Huo, C. Xu, Z. Ji, R. Liu, B. Liu, Y. Li, and F. Feng, "High-precision electrical impedance tomography data acquisition system for brain imaging," *IEEE Sensors J.*, vol. 18, no. 14, pp. 5974–5984, Jul. 2018.

HANG MA received the B.S. and M.S. degrees in biomedical engineering from Fourth Military Medical University, Xi'an, China, in 2013 and 2016, respectively, where he is currently pursuing the Ph.D. degree under the Supervision of Professor F. Fu. His research interest includes biosensor system design.

HAOTING LI received the B.S. and M.S. degrees in biomedical engineering from Fourth Military Medical University, Xi'an, China, in 2014 and 2017, respectively, where he is currently pursuing the Ph.D. degree under the Supervision of Professor F. Fu. His research interest includes EIT reconstruction algorithm.

XUECHAO LIU received the B.S. degree in communication engineering from the Ocean University of China, Qing Dao, China, in 2016. She is currently pursuing the B.S. degree with Fourth Military Medical University under the Supervision of Professor F. Fu. His research interest includes EIT reconstruction algorithm.

WEICHEN LI received the B.S. degree in automatic control from Tianjin University, Tianjin, China, in 2012, and the M.S. degree in biomedical engineering from Fourth Military Medical University, Xi'an, China, in 2015, where he is currently pursuing the Ph.D. degree under the Supervision of Professor X. Shi. His research interests include biomedical electrical instrumentation, biomedical signal processing, and analysis of instrumentation noise.

JUNYING XIA received the B.S., M.S., and Ph.D. degrees in instrument science and technology from the National University of Defense Technology, Changsha, China, in 2004, 2006, and 2012, respectively. He is currently a Lecturer with the Department of Biomedical Engineering, Fourth Military Medical University. His current research interest includes analysis and measurement of biological signals.

BENYUAN LIU was born in Shanxi, China, in 1985. He received the M.S. and Ph.D. degrees in science and technology from the Automatic Target Recognition Laboratory, National University of Defense Technology, Changsha, China, in 2009 and 2015, respectively. He is currently a Lecturer with the Department of Biomedical Engineering, Fourth Military Medical University. His research interests include electrical impedance tomography (EIT), inverse problems, and adaptive waveform optimization.

XUETAO SHI was born in China, in 1973. He received the B.S., M.S., and Ph.D. degrees in biomedical engineering from Fourth Military Medical University, Xi'an, China, in 1995, 2001, and 2006, respectively, where he is currently a Professor with the Department of Biomedical Engineering. His current research interests include the measurement and analysis of dielectric properties of tissues, bio-impedance measurement, and imaging monitoring by electrical impedance tomography.

XIUZHEN DONG (M'00) was born in China, in 1945. She received the B.S. degree in automatic control from Harbin Military Engineering University, Harbin, China, in 1968. Since 1994, she has been a Professor at Fourth Military Medical University, Xi'an, China, where she has also been a Doctoral Advisor, since 1998. She is the author or coauthor of more than 200 papers published in international journals and conferences. Her current research interests include electrical impedance tomography, and biomedical signal detection and processing.

FENG FU received the B.S., M.S., and M.D. degrees in biomedical engineering from Fourth Military Medical University, Xi'an, China, in 1993, 1996, and 1999, respectively, where he is currently a Professor with the Department of Biomedical Engineering. His current research interests include electrical impedance measurement and imaging.

• • •